Sliding Mode Based Droop Control Strategies for Parallel-Connected Inverters in Railway Vehicles

Aline Cristiane Buzzi*, Gian Paolo Incremona*, Patrizio Colaneri*, Andrea Dolcini** and Angelo Colombo**

Abstract— **This paper deals with the design of sliding mode based droop control strategies for parallel-connected inverters in railway vehicles. Indeed, the presence of auxiliary devices, which can be connected and disconnected at any time instant, makes the introduction of parallel modules an efficient solution. Among the possible techniques, droop control represents an efficient and easy-to-implement approach. However, each inverter is affected by load variations, nonlinearities and unavoidable modelling uncertainties, thus making the use of sliding mode controllers perfectly adequate for this kind of application. More specifically, relying on a sliding surface designed on the basis of a voltage-current droop characteristic, two second order sliding mode (SOSM) control algorithms, belonging to the class of Super-Twisting and Suboptimal SOSM control, are proposed.**

I. Introduction

Nowadays, railway vehicles are considered by far the most efficient means of transportation from the point of view of energy consumption and therefore this is a strategic sector in the transportation industry [1], [2]. The need to decrease energy consumption in order to be sustainable and more profitable in the future has paved the way for new control methods and architectures for trains. These methods differ on the basis of certain factors: some of them are operator based, which require upgrade in the vehicle technology, while other techniques are control based [3]. For example, in order to reduce energy, an operator can deploy more valuable rolling stock by using more energy efficient engines or streamlining. Also, the operator may work to better match the capacities of the trains with the demand and deploy measures concerning heating, cooling, lightning and other auxiliary services.

As for auxiliary devices, they are typically supplied by inverters located inside the train carriages and a widely spread configuration relies on a centralized control architecture. However, this scheme has the problem to be not very efficient in the low power range and the Voltage Source Converters (VSCs) can be often expensive and bulky. Then, a valid alternative is that of using a decentralized architecture with parallel-connected inverters, each one of them is capable to manage a fraction of the full power [4], [5]. The parallel connection of inverters has indeed the main advantages of modularity and flexibility, allowing disconnection of some units on the basis of the required power level. As a consequence this architecture is more efficient in case of low power range and implies lower volume, weight and costs.

In the literature the so-called droop control is considered an effective decentralized strategy to cope with this type of systems [6]–[8]. More specifically, the parallel architecture is typical of islanded microgrids where power converters have to satisfy power requirements while fulfilling voltage stability and frequency constraints. The scope of droop control is to make multi-inverters share loads according to their power rating. In [9], for instance, the inverter output characteristic is changed relying on a virtual impedence control and active and reactive power-voltage droop functions are employed. Further improvements are introduced in [4] and then in [10], where voltage-current droop control under synchronous reference frame is proposed, with advantages in terms of computational burden and decoupling of voltages and currents. Typically, Proportional-Integral (PI) controllers are adopted to regulate the system, while other solutions, always applied for microgrids case studies, are related to consensus algorithms or optimal control strategies, as reported in [11]–[13].

Since the presence of VSCs can produce undesired harmonics and the presence of coupling effects and modelling uncertainties is unavoidable, robust control strategies are essential for this type of applications. Among the possibilities, Sliding Mode Control (SMC) is a powerful solution, which perfectly fits the control problem to solve [14]. Relying on a discontinuous control action, generated on the basis of the so-called sliding variable typically related to the required performance of the plant, interesting robustness features of the controlled system can be achieved. If on one hand the main drawback is the so-called chattering phenomenon, on the other hand Higher-Order Sliding Mode (HOSM) controllers are a valid solution to alleviate it by confining the discontinuity of the control law into the derivative of the real control input [15]–[18]. In this paper, inspired by [10], a sliding variable, which relies on a voltage-current droop characteristic, is designed in order to enable the current sharing objective, and two second-order SMCs of Super-Twisting and Suboptimal type are introduced to solve the problem at hand.

This is the final version of the accepted paper submitted for inclusion in the Proceedings of the European Control Conference, Jul., 2020, DOI: 10.23919/ECC51009.2020.9143784. This work has been partially supported by the Italian Ministry for Research in the framework of the 2017 Program for Research Projects of National Interest (PRIN), Grant no. 2017YKXYXJ.

*Aline Cristiane Buzzi, Gian Paolo Incremona and Patrizio Colaneri are with the Dipartimento di Elettronica, Informazione e Bioingegneria, Politecnico di Milano, Piazza Leonardo da Vinci 32, 20133 Milan, Italy (e-mail: alinecristiane.buzzi@mail.polimi.it, gianpaolo.incremona@polimi.it, patrizio.colaneri@polimi.it).

**Andrea Dolcini and Angelo Colombo are with the rail transport company Alstom SESTO, Via Fosse Ardeatine, 120, 20099 Sesto San Giovanni, Milan, Italy (e-mail: andrea.dolcini@alstomgroup.com, angelo.colombo@alstomgroup.com).

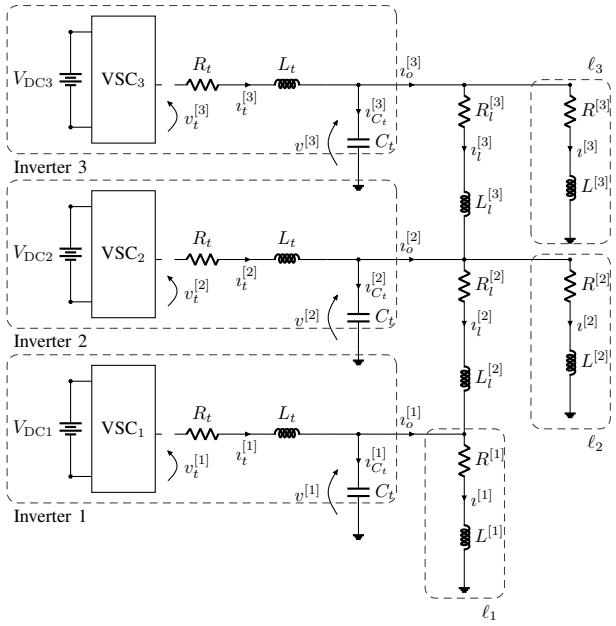

Fig. 1. Single-line diagram of three parallel-connected inverters

The paper is organized as follows. After some preliminaries on the train structure and the operative mode in Section II, the model is introduced in Section III. The proposed algorithms are presented in Section IV, while simulations, carried out on a realistic setup, are illustrated in Section V. In Section VI some conclusions are gathered.

II. Train architecture

In this section, for the readers' convenience, the architecture of a parallel multi-inverters system is illustrated.

Let us denote as ℓ_i, $i = 1, \ldots, n$ the auxiliary loads, fed by parallel voltage source converters indicated as VSC$_i$. The parallel configuration allows one to achieve more flexibility in order to add or remove elements from time to time. Figure 1 illustrates in detail the schematic single-line diagram of a system composed, for the sake of simplicity, of three parallel-connected inverters. The basic element of each inverter subsystem is given by a direct current (dc) voltage source $V_{\mathrm{DC}i}$. The latter is interfaced with the rest of the grid through three components: the VSC, a filter and a capacitor. Typically the VSC is a pulse with modulation (PWM) converter, which transforms the dc to alternate current (ac). On the other hand, the resistive-inductive filter $R_t L_t$ extracts the fundamental frequency of the VSC output voltage. The capacitor C_t determines instead the output voltage of the ith subsystem indicated with $v_{C_t}^{[i]}$, as well as the corresponding output current, namely $\imath_o^{[i]}$. Each subsystems is then connected to a local three-phase parallel resistive-inductive $R^{[i]}L^{[i]}$ load, and, apart from the last one, they are connected each other through a resistive-inductive $R_l^{[i]}L_l^{[i]}$ line impedance.

III. Problem Formulation

In this section, the model of the train parallel-inverters is described and the control problem is introduced.

A. Train inverters model

Consider now Figure 1 where three parallel-connected inverters are illustrated. Applying the Kirchhoff's voltage and current laws, in the so-called abc-frame, the model is

$$\left.\begin{aligned}\tfrac{d\imath_t^{[1]}}{dt} &= \tfrac{1}{L_t}\left(v_t^{[1]} - v_{C_t}^{[1]} - R_t\imath_t^{[1]}\right)\\ \tfrac{dv_{C_t}^{[1]}}{dt} &= \tfrac{1}{C_t}\left(\imath_t^{[1]} - \imath^{[1]} + \imath_l^{[2]}\right)\end{aligned}\right\},\quad \mathrm{VSC}_1$$
$$\tfrac{d\imath^{[1]}}{dt} = \tfrac{1}{L^{[1]}}\left(v_{C_t}^{[1]} - R^{[1]}\imath^{[1]}\right),\quad \ell_1$$
$$\left.\begin{aligned}\tfrac{d\imath_t^{[2]}}{dt} &= \tfrac{1}{L_t}\left(v_t^{[2]} - v_{C_t}^{[2]} - R_t\imath_t^{[2]}\right)\\ \tfrac{dv_{C_t}^{[2]}}{dt} &= \tfrac{1}{C_t}\left(\imath_t^{[2]} - \imath^{[2]} - \imath_l^{[2]} + \imath_l^{[3]}\right)\end{aligned}\right\},\quad \mathrm{VSC}_2$$
$$\tfrac{d\imath^{[2]}}{dt} = \tfrac{1}{L^{[2]}}\left(v_{C_t}^{[2]} - R^{[2]}\imath^{[2]}\right),\quad \ell_2 \qquad (1)$$
$$\tfrac{d\imath_l^{[2]}}{dt} = \tfrac{1}{L_l^{[2]}}\left(v_{C_t}^{[2]} - v_{C_t}^{[1]} - R_l^{[2]}\imath_l^{[2]}\right),\quad l_{1\backslash 2}$$
$$\left.\begin{aligned}\tfrac{d\imath_t^{[3]}}{dt} &= \tfrac{1}{L_t}\left(v_t^{[3]} - v_{C_t}^{[3]} - R_t\imath_t^{[3]}\right)\\ \tfrac{dv_{C_t}^{[3]}}{dt} &= \tfrac{1}{C_t}\left(\imath_t^{[3]} - \imath^{[3]} - \imath_l^{[3]}\right)\end{aligned}\right\},\quad \mathrm{VSC}_3$$
$$\tfrac{d\imath^{[3]}}{dt} = \tfrac{1}{L^{[3]}}\left(v_{C_t}^{[3]} - R^{[3]}\imath^{[3]}\right),\quad \ell_3$$
$$\tfrac{d\imath_l^{[3]}}{dt} = \tfrac{1}{L_l^{[3]}}\left(v_{C_t}^{[3]} - v_{C_t}^{[2]} - R_l^{[3]}\imath_l^{[3]}\right),\quad l_{2\backslash 3}$$

where $\imath_t^{[i]}, \imath^{[i]}, \imath_l^{[i]}, v_t^{[i]}, v_{C_t}^{[i]}$ are 3×1 column vectors (one entry for each phase) representing the VSC output current, the load current, the line current, the VSC output voltage and the capacitor voltage, respectively. The inverter output current of interest is instead given by

$$\imath_o^{[i]} = \imath_t^{[i]} - \imath_{C_t}^{[i]}\,. \qquad (2)$$

Note that the dependence of all the variables on time t is omitted, for the sake of simplicity.

In order to achieve a state model of system (1) in a suitable form for control design, each three-phase variable $s \in \left\{\imath_t^{[i]}, \imath_l^{[i]}, \imath^{[i]}, v_t^{[i]}, v_{C_t}^{[i]}\right\}$ can be transferred to the synchronous rotating dq-frame, with $S \in \left\{I_t^{[i]}, I_l^{[i]}, I^{[i]}, V_t^{[i]}, V_{C_t}^{[i]}\right\}$ being the dq variables, by using the Clarke's and Park's transformations. Hence, the so-called state-space model of (1)–(2), extended to n parallel-connected inverters, is

$$\begin{cases}\dot{x}^{[i]} = Ax^{[i]} + Bu^{[i]} + M\left(w^{[i]} - w^{[i+1]} + d^{[i]}\right)\\ y^{[i]} = C_1 x^{[i]}\\ \dot{w}^{[i]} = E^{[i]}w^{[i]} + G^{[i]}C_2\left(x^{[i]} - x^{[i-1]}\right)\\ \dot{d}^{[i]} = F^{[i]}d^{[i]} + H^{[i]}C_2 x^{[i]}\end{cases} \qquad (3)$$

where $i = 1, \ldots, n$, with $w^{[n+1]} = 0$ and $x^{[0]} = 0$,

$$x^{[i]} = \begin{bmatrix} I_{td}^{[i]} \\ I_{tq}^{[i]} \\ V_{C_t d}^{[i]} \\ V_{C_t q}^{[i]} \end{bmatrix},\ u^{[i]} = \begin{bmatrix} V_{td}^{[i]} \\ V_{tq}^{[i]} \end{bmatrix},\ d^{[i]} = \begin{bmatrix} I_d^{[i]} \\ I_q^{[i]} \end{bmatrix},\ w^{[i]} = \begin{bmatrix} I_{ld}^{[i]} \\ I_{lq}^{[i]} \end{bmatrix} \qquad (4)$$

while the matrices are

$$A = \begin{bmatrix} -\frac{R_t}{L_t} & \omega_0 & -\frac{1}{L_t} & 0 \\ -\omega_0 & -\frac{R_t}{L_t} & 0 & -\frac{1}{L_t} \\ \frac{1}{C_t} & 0 & 0 & \omega_0 \\ 0 & \frac{1}{C_t} & -\omega_0 & 0 \end{bmatrix}, \; B = \begin{bmatrix} \frac{1}{L_t} & 0 \\ 0 & \frac{1}{L_t} \\ 0 & 0 \\ 0 & 0 \end{bmatrix},$$

$$C_1 = \begin{bmatrix} 1 & 0 & 0 & \omega_0 C_t \\ 0 & 1 & -\omega_0 C_t & 0 \end{bmatrix},$$

$$C_2 = \begin{bmatrix} 0 & 0 & 1 & 0 \\ 0 & 0 & 0 & 1 \end{bmatrix}, \; M = \begin{bmatrix} 0 & 0 \\ 0 & 0 \\ -\frac{1}{C_t} & 0 \\ 0 & -\frac{1}{C_t} \end{bmatrix},$$

$$F^{[i]} = \begin{bmatrix} -\frac{R^{[i]}}{L^{[i]}} & \omega_0 \\ -\omega_0 & -\frac{R^{[i]}}{L^{[i]}} \end{bmatrix}, \; H^{[i]} = \begin{bmatrix} \frac{1}{L^{[i]}} & 0 \\ 0 & \frac{1}{L^{[i]}} \end{bmatrix},$$

$$E^{[i]} = \begin{bmatrix} -\frac{R_l^{[i]}}{L_l^{[i]}} & \omega_0 \\ -\omega_0 & -\frac{R_l^{[i]}}{L_l^{[i]}} \end{bmatrix}, \; G^{[i]} = \begin{bmatrix} \frac{1}{L_l^{[i]}} & 0 \\ 0 & \frac{1}{L_l^{[i]}} \end{bmatrix}. \tag{5}$$

It can be observed that, while matrices A, B, C_1, C_2 and M are independent of the ith VSC, matrices $F^{[i]}$, $H^{[i]}$, $E^{[i]}$ and $G^{[i]}$ depend on the parameters of the ith load and on those of the line between the ith and $(i+1)$th inverter ($l_{i\backslash(i+1)}$). Furthermore, the vector $d^{[i]}$ can be considered as a disturbance term for which the following assumption holds.

Assumption 1: All the state variables are measurable and the current loads $d^{[i]}$ are unknown and bounded, of class C and Lipshitz continuous. □

As for the $R^{[i]}L^{[i]}$ load, having in mind the field implementation of the proposal, it is typically expressed in terms of apparent power and power factor, namely $\cos\phi$. Alternatively, it is directly indicated in terms of active ($P^{[i]}$) and reactive ($Q^{[i]}$) powers, given by

$$P^{[i]} = \frac{3}{2}\left(V_{C_t d}^{[i]} I_d^{[i]} + V_{C t q}^{[i]} I_q^{[i]}\right) \tag{6}$$

$$Q^{[i]} = \frac{3}{2}\left(V_{C_t q}^{[i]} I_d^{[i]} - V_{C_t d}^{[i]} I_q^{[i]}\right). \tag{7}$$

Since the voltage $V_{C_t q}^{[i]}$ has to be forced to zero in order to stabilize the system at the rated frequency with zero phase delay, active and reactive powers can be decoupled and expressed only as functions of $V_{C_t d}^{[i]}$. Finally, having in mind a reactive-inductive load, it can be expressed as

$$R^{[i]} = \frac{P^{[i]}(V_{C_t d}^{[i]})^2}{(P^{[i]})^2 + (Q^{[i]})^2} \tag{8}$$

$$L^{[i]} = \frac{Q^{[i]}(V_{C_t d}^{[i]})^2}{\omega_0\left[(P^{[i]})^2 + (Q^{[i]})^2\right]}. \tag{9}$$

B. The current sharing control problem

We are now in a position to introduce the current sharing control problem. Having in mind the train application, where loads can be dropped or added at any time instant depending on different needs, the objective is to continuously share the load among all the inverters. Assuming that the quadrature component $V_{C_t q}^{[i]}$ is steered to zero, we can formulate the following definition of "direct current load sharing" [11].

Definition 1: Direct current load sharing is achieved if the overall direct component of the load current is equally shared among the inverters, i.e.,

$$I_{od} = \mathbb{1}_n I_{od}^* \quad I_{od}^* = \frac{1}{n}\mathbb{1}_n^\top I_d \in \mathbb{R} \tag{10}$$

where I_{od}, $I_d \in \mathbb{R}^n$ are the inverters' output and load currents, while $\mathbb{1}_n \in \mathbb{R}^n$ is the vector containing all ones. □

Hence, the control problem to solve is the following one.

Control Problem 1: Given system (3)–(5), design a control law such that $V_{C_t q}^{[i]}$ and $V_{C_t d}^{[i]}$ are regulated in a neighborhood of zero and $V_{C_t d}^*$, respectively, thus enabling current sharing in spite of connection and disconnection of unknown bounded loads.

IV. The Proposed Sliding Mode based Droop Control Strategies

In this section, the previous control problem is solved by introducing sliding mode based droop control algorithms. Inspired by [10], the so-called sliding variable is designed as a voltage-current droop function. Before introducing the controllers, the following assumption is also required.

Assumption 2: The voltage reference $V_{C_t d}^*$ is of class C^2 and with first time derivative Lipschitz continuous, while, $V_{C_t q}^* = 0$. □

A. Design of the sliding manifold

Considering system (3) separately for the direct and quadrature component, and assuming to have small line impedence, relying on the Thévenin's theorem, it is possible to verify that in steady-state among parallel branches it holds

$$\frac{I_{t\nu}^{[i]}}{I_{t\nu}^{[i+1]}} = \frac{R_{v\nu}^{[i+1]}}{R_{v\nu}^{[i]}}, \quad i = 1, \ldots, n-1 \tag{11}$$

where $R_{v\nu}^{[i]}$, $\nu \in \{d, q\}$ are the so-called virtual resistances of the inverters. Considering the references $V_{C_t d}^*$ and $V_{C_t q}^*$ equal for each inverter, the relationship (11) can be written also in terms of active and reactive powers. Hence, one can write the following droop strategy

$$\begin{aligned} I_{td}^{[i]*} &= I_{t0d}^* - \tfrac{1}{R_{vd}^{[i]}}\left(V_{C_t d}^{[i]} - V_{C_t d}^*\right) \\ I_{tq}^{[i]*} &= I_{t0q}^* - \tfrac{1}{R_{vq}^{[i]}}\left(V_{C_t q}^{[i]} - V_{C_t q}^*\right) \end{aligned} \tag{12}$$

where $I_{t\nu}^{[i]*}$ are the direct and quadrature current references while $I_{t0\nu}^*$ are the nominal values. Analyzing the droop relationships in (12), the direct component is responsible to adapt the value of the current reference relying on the droop characteristics, while the quadrature component plays the important role to maintain the frequency at the rated value. Furthermore, each inverter can be regulated without requiring information from the others.

Since the input of the ith inverter is given by the voltages $V_{td}^{[i]}$, $V_{tq}^{[i]}$ and the droop characteristics determine the current

references, the sliding variables $\sigma^{[i]} = \left[\sigma_d^{[i]}, \sigma_q^{[i]}\right]^\top$ are designed as

$$\begin{aligned}\sigma_d^{[i]} &= \tfrac{1}{R_{\mathrm{v}d}^{[i]}}\left(V_{C_t d}^* - V_{C_t d}^{[i]}\right) + \left(I_{t0d}^* - I_{td}^{[i]}\right)\\ \sigma_q^{[i]} &= \tfrac{1}{R_{\mathrm{v}q}^{[i]}}\left(V_{C_t q}^* - V_{C_t q}^{[i]}\right) + \left(I_{t0q}^* - I_{tq}^{[i]}\right)\ .\end{aligned} \tag{13}$$

Relying on system (3) and computing the first time derivative of (13), the corresponding relative degree (i.e., the minimum order of the time derivative $\sigma^{(r)[i]}$ where the control input explicitly appears) is equal to 1. Hence, a first order sliding mode naturally applies. However, the main drawback of sliding mode control is the so-called chattering phenomenon. Among the possible solutions, HOSM control algorithms are the most successful techniques. In the following two different approaches are discussed, that is the Super-Twisting Sliding Mode (STSM) algorithm and the Suboptimal Second-Order Sliding Mode (SSOSM) control.

B. STSM control algorithm

One of the main features of STSM control is that it can be applied only to relative degree-one system. By virtue of the choice of the sliding variables (13), the considered first order system becomes

$$\dot{\sigma}^{[i]} = f_1^{[i]}(x^{[i]}, d^{[i]}, w^{[i]}) + g u^{[i]} \tag{14}$$

where

$$f_1^{[i]} = \begin{bmatrix} -\frac{1}{R_{\mathrm{v}d}^{[i]} C_t} + \frac{R_t}{L_t} & -\omega_0 & \frac{1}{L_t} & -\frac{\omega_0}{R_{\mathrm{v}d}^{[i]}} \\ \omega_0 & -\frac{1}{R_{\mathrm{v}q}^{[i]} C_t} + \frac{R_t}{L_t} & \frac{\omega_0}{R_{\mathrm{v}q}^{[i]}} & \frac{1}{L_t} \end{bmatrix} x^{[i]} + \\ + \begin{bmatrix} \frac{1}{R_{\mathrm{v}d}^{[i]} C_t} & 0 \\ 0 & \frac{1}{R_{\mathrm{v}q}^{[i]} C_t} \end{bmatrix} \left(d^{[i]} + w^{[i]} - w^{[i+1]}\right) \tag{15}$$

$$g = \begin{bmatrix} -\frac{1}{L_t} & 0 \\ 0 & -\frac{1}{L_t} \end{bmatrix} \tag{16}$$

are uncertain and bounded function such that the following assumption holds.

Assumption 3: There exist positive constants $F_{1\nu}^{[i]}$, $F_{2\nu}^{[i]}$ and $G_{1\nu\min}$, $G_{1\nu\max}$, with $\nu \in \{d, q\}$, such that

$$|f_{1\nu}^{[i]}| \le F_{1\nu}^{[i]} \tag{17}$$

$$\left|\frac{\mathrm{d}f_{1\nu}^{[i]}}{\mathrm{d}t}\right| \le F_{2\nu}^{[i]} \tag{18}$$

$$-G_{1\nu\max} \le g_\nu \le -G_{1\nu\min} < 0\ , \tag{19}$$

with $f_{1\nu}^{[i]}$ and g_ν being the direct and quadrature components of (15) and (16), respectively. □

The STSM control is instead given by

$$\begin{aligned} V_{t\nu}^{[i]} &= u_{1\nu}^{[i]} + u_{2\nu}^{[i]}\\ u_{1\nu}^{[i]} &= \alpha_{1\nu}^{[i]} |\sigma_\nu^{[i]}|^{\frac{1}{2}} \operatorname{sgn}(\sigma_\nu^{[i]})\\ \dot{u}_{2\nu}^{[i]} &= \alpha_{2\nu}^{[i]} \operatorname{sgn}(\sigma_\nu^{[i]}) \end{aligned} \tag{20}$$

where $\alpha_{1\nu}^{[i]}$ and $\alpha_{2\nu}^{[i]}$ are positive constants chosen in order to dominate the uncertain terms affecting the system. Note that the control input directly fed into the plant is continuous, thus enabling a chattering alleviation property of the algorithm.

C. SSOSM control algorithm

Another possibility to solve the control problem at hand is the so-called SSOSM control algorithm. In this case, in order to achieve similar chattering alleviation property as for the STSM control, an artificially increment of the relative degree is operated. More specifically, introducing auxiliary variables $z_{(j+1)\nu}^{[i]} = \sigma_\nu^{(j)[i]}$, $j = 0, 1$, the so-called second-order auxiliary system results

$$\begin{aligned} \dot{z}_{1\nu}^{[i]} &= z_{2\nu}^{[i]}\\ \dot{z}_{2\nu}^{[i]} &= f_{2\nu}^{[i]}(x^{[i]}, d^{[i]}, w^{[i]}) + g_\nu \mu_\nu^{[i]}\\ \dot{V}_{t\nu}^{[i]} &= \mu_\nu^{[i]} \end{aligned} \tag{21}$$

where $f_{2\nu}^{[i]} = \frac{\mathrm{d}f_{1\nu}^{[i]}}{\mathrm{d}t}$ and g_ν as in (16), which are bounded by virtue of Assumption 3. The so-called SSOSM control law is given by

$$\mu_\nu^{[i]} = \gamma^{[i]} \alpha_{3\nu}^{[i]} \operatorname{sgn}\left(z_{1\nu}^{[i]} - \tfrac{1}{2} z_{\max}\right) \tag{22}$$

$$\gamma^{[i]} \in (0,\, 1) \cap \left(0,\, \tfrac{3G_{1\nu\min}}{G_{1\nu\max}}\right) \tag{23}$$

$$\alpha_{3\nu}^{[i]} > \max\left(\tfrac{F_{2\nu}^{[i]}}{\gamma^{[i]} G_{1\nu\min}},\, \tfrac{4F_{2\nu}^{[i]}}{3G_{1\nu\min} - \gamma^{[i]} G_{1\nu\max}}\right) \tag{24}$$

where $z_{\max}$ are the extremal values of $z_{1\nu}^{[i]}$, computed using a peak detector as discussed for instance in [18].

D. Convergence argumentation

Referring to [14, Chapter 2], and taking into account the features of the considered parallel multi-inverters system, one can prove that STSM and SSOSM controllers make the sliding variables, $\sigma_\nu^{[i]}$, converge to zero in a finite time. On the other hand, the controlled voltages converge in a neighborhood of their reference values, which depends on the parameters of lines and loads, and on the selected virtual resistances. Furthermore, we also refer to [14] for providing some rules to practitioners interested in implementing the proposed sliding mode approaches.

V. Case Study

In this section the proposed HOSM control strategies are assessed on realistic simulator implemented in MATLAB–Sim Power Systems with data provided by Alstom for a train with 4 inverters and 7 loads.

A. Settings and scenario

The electric parameters of the system and the involved powers are reported in Table I. All the loads can be connected and disconnected by means of a dedicated switch and each VSC is fed by 600 V not-reversible voltage source. All the inverters are reasonably assumed to be equal. This assumption is not restrictive and, suitably tuning the control parameters, the proposal is valid even in case of heterogeneous subsystems. Inverters 1, 3 and 4 can be directly connected to their single loads ℓ_1, ℓ_3 and ℓ_4, while inverter 2 can supply four loads ℓ_{2j}, $j = 1, 2, 3, 4$ connected each other through three lines denoted as $l_{2_{j\setminus(j+1)}}$. The first module is denoted as "master" inverter and is connected to the grid when the

TABLE I

INVERTERS, LINES AND LOADS PARAMETERS

$i = 1, \ldots, 4$		
VSC$_i$	V_{DC_i}	600 V
	R_t	1 mΩ
	L_t	210 µH
	C_t	2.4 mF
	ω_0	50 Hz
$l_{1\backslash 2}$	$R_l^{[2]}$	7.5 mΩ
	$L_l^{[2]}$	12.6 mH
ℓ_1	$R^{[1]}$	1.45 Ω
	$L^{[1]}$	3.1 mH

$l_{2_{1\backslash 2}}$	$R_{l1}^{[3]}$	7.1 mΩ	$l_{2_{3\backslash 4}}$	$R_{l3}^{[3]}$	4.9 mΩ
	$L_{l1}^{[3]}$	12 mH		$L_{l3}^{[3]}$	8.2 mH
ℓ_{21}	$R_1^{[2]}$	1.79 Ω	ℓ_{23}	$R_3^{[2]}$	1.25 Ω
	$L_1^{[2]}$	4 mH		$L_3^{[2]}$	2.7 mH
$l_{2_{2\backslash 3}}$	$R_{l2}^{[3]}$	7.5 mΩ	$l_{2_{4\backslash 5}}$	$R_l^{[3]}$	7.9 mΩ
	$L_{l2}^{[3]}$	12.6 mH		$L_l^{[3]}$	13.2 mH
ℓ_{22}	$R_2^{[2]}$	1.03 Ω	ℓ_{24}	$R_4^{[2]}$	1.25 Ω
	$L_2^{[2]}$	2 mH		$L_4^{[2]}$	2.7 mH

$l_{3\backslash 4}$	$R_l^{[4]}$	7.5 mΩ
	$L_l^{[4]}$	12.6 mH
ℓ_3	$R^{[3]}$	1.86 Ω
	$L^{[3]}$	4.1 mH
ℓ_4	$R^{[4]}$	1.48 Ω
	$L^{[4]}$	3.2 mH

TABLE II

SCENARIO: INVERTERS INITIALIZATION PHASE (GRAY), INVERTERS/LOADS POWER ON (LIGHT GRAY) AND POWER OFF (DARK GRAY) INTERVALS

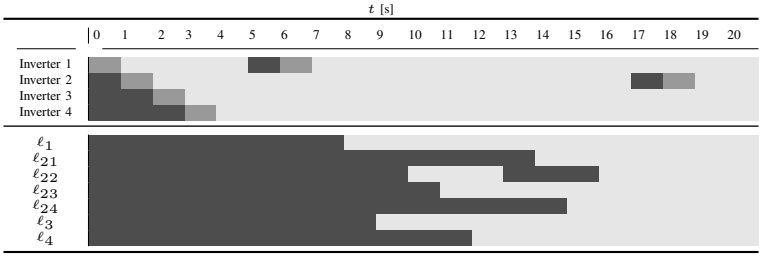

TABLE III

CONTROL PARAMETERS

$i = 1, \ldots, 4;\ \nu \in \{d, q\}$		
	$V^*_{C_t d}$	326.6 V
	$V^*_{C_t q}$	0 V
	$R_{\nu\nu}^{[i]}$	80×10^{-3} Ω
STSM	$\alpha_{1\nu}^{[i]}$	1
	$\alpha_{2d}^{[i]}$	670.5
	$\alpha_{2q}^{[i]}$	1
SSOSM	$\gamma^{[i]}$	1
	$\alpha_{3d}^{[i]}$	670.5
	$\alpha_{3q}^{[i]}$	1

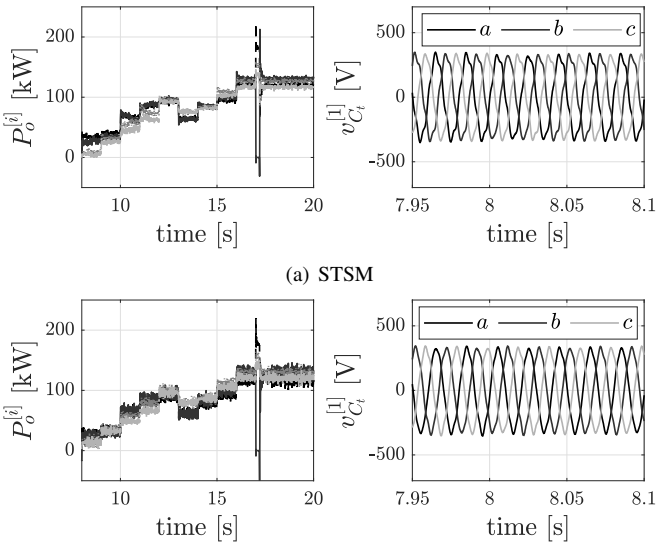

(a) STSM

(b) SSOSM

Fig. 2. Powers (left) from the inverters ($i = 1, \ldots, 4$), and three-phase voltages (right) on the 1st capacitor ($v_{C_t}^{[1]}$) when the proposed sliding mode controllers are used. (a) STSM. (b) SSOSM

corresponding capacitor voltage $V_{C_t}^{[1]}$ reaches a stable value around 400 V (initialization phase). All the other inverters are then connected shifted in time of 1 s. After 3.5 s, all inverters are turned on. At the time instant 5 s inverter 1 is turned off and activated after 1 s. Finally, from the time instant 8 s the loads are inserted according to the sequence reported in Table II. As for the controllers, the virtual resistances and gains are reported in Table III. The total simulation lasts 20 s with sampling time equal to 5 µs.

B. Results

When the loads start to connect (8 s), the condition of "direct current load sharing" is enabled. Figure 2 shows the evolution of the output powers ($P_o^{[i]}$) of the inverters (left) and the three-phase voltages (right) only on the 1st capacitor ($v_{C_t}^{[1]}$), as an example. The latter appears a smooth three-phase sinusoidal signal and at time 8 s the connection of load ℓ_1 does not affect the voltages, thus assessing the robustness of the proposals in front of units connection and disconnection.

C. Comparison

To further assess the proposals, they are compared with droop-control having Proportion-Integral regulation of the inverter currents (DC [10]) and with a First-Order Sliding Mode (FOSM) control. For a quantitative comparison the Total Harmonic Distortion (THD) of the load voltages, and the root-mean-square values of the dc-link voltages (V_{DCrms}) are computed. For these indices, then the average among all the loads and inverters (namely $\mathrm{m}(\cdot)$) is achieved and

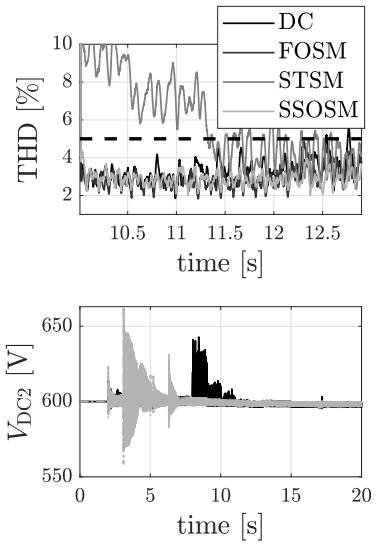

Fig. 3. Total Harmonic Distortion (THD) of the load voltage (top) when ℓ_{22} is connected, and the dc-link voltage V_{DC2} (bottom)

TABLE IV
PERFORMANCE INDICES

	m(THD) [%]	m(V_{DCrms}) [V]
DC [10]	2.032	599.26
FOSM	2.036	599.06
STSM	4.47	599.09
SSOSM	2.046	599.01

reported in Table IV. As for the THD, the performance is similar for all the controllers apart from that of STSM. This aspect can be noticed, for instance, in Figure 3 (top) for load ℓ_{22}. Indeed, in our tests, STSM is more sensitive to load variations, presenting greater voltage distortions than those visible when using the other methods. During the interval when the load is supplied, the best performance over time is instead guaranteed by the SSOSM algorithm, which is always below the maximum allowed threshold (5%). As for the rms-values of the dc-link voltages, although they are similar for all the algorithms, in Figure 3 (bottom) the DC solution (black lines) is visibly more sensitive to connection and disconnection of inverters and loads (see, e.g., after the time instant $8\,\mathrm{s}$).

VI. Conclusions

In this paper sliding mode based droop control strategies have been proposed for parallel-connected inverters in railway vehicles. The model of the system, which is coupled due to the presence of line impedances among the inverters, has been formulated. A STSM control and a SSOSM one have been designed and discussed. Finally, realistic simulation results, based on real data, have been illustrated and a comparative study with PI-based DC and FOSM control has been performed. Future works will attempt to introduce an adaptation mechanism to cope with eventually unknown bounds of the uncertain terms affecting the system.

References

[1] A. Albrecht, P. Howlett, P. Pudney, X. Vu, and P. Zhou, "The key principles of optimal train control–part 1: Formulation of the model, strategies of optimal type, evolutionary lines, location of optimal switching points," *Transportation Research Part B: Methodological*, vol. 94, pp. 482–508, Dec. 2016.

[2] Q. Gu, T. Tang, F. Cao, and Y. D. Song, "Energy-efficient train operation in urban rail transit using real-time traffic information," *IEEE Transactions on Intelligent Transportation Systems*, vol. 15, no. 3, pp. 1216–1233, Feb. 2014.

[3] H. Farooqi, G. P. Incremona, and P. Colaneri, "Railway collaborative ecodrive via dissension based switching nonlinear model predictive control," *European Journal of Control*, Nov. 2019.

[4] J. M. Guerrero, J. Matas, L. Garcia de Vicuna, M. Castilla, and J. Miret, "Decentralized control for parallel operation of distributed generation inverters using resistive output impedance," *IEEE Transactions on Industrial Electronics*, vol. 54, no. 2, pp. 994–1004, Apr. 2007.

[5] J. C. Vasquez, J. M. Guerrero, M. Savaghebi, J. Eloy-Garcia, and R. Teodorescu, "Modeling, analysis, and design of stationary-reference-frame droop-controlled parallel three-phase voltage source inverters," *IEEE Transactions on Industrial Electronics*, vol. 60, no. 4, pp. 1271–1280, Apr. 2013.

[6] W. Yao, M. Chen, J. Matas, J. M. Guerrero, and Z. Qian, "Design and analysis of the droop control method for parallel inverters considering the impact of the complex impedance on the power sharing," *IEEE Transactions on Industrial Electronics*, vol. 58, no. 2, pp. 576–588, Feb. 2011.

[7] J. Kim, J. M. Guerrero, P. Rodriguez, R. Teodorescu, and K. Nam, "Mode adaptive droop control with virtual output impedances for an inverter-based flexible ac microgrid," *IEEE Transactions on Power Electronics*, vol. 26, no. 3, pp. 689–701, Mar. 2011.

[8] C.-T. Lee, C.-C. Chu, and P.-T. Cheng, "A new droop control method for the autonomous operation of distributed energy resource interface converters," *IEEE Transactions on Power Electronics*, vol. 28, no. 4, pp. 1980–1993, Apr. 2013.

[9] K. De Brabandere, B. Bolsens, J. Van den Keybus, A. Woyte, J. Driesen, and R. Belmans, "A voltage and frequency droop control method for parallel inverters," *IEEE Transactions on Power Electronics*, vol. 22, no. 4, pp. 1107–1115, Jul. 2007.

[10] M. Li, Y. Gui, Z. Jin, Y. Guan, and J. M. Guerrero, "A synchronous-reference-frame I-V droop control method for parallel-connected inverters," in *Proc. 2018 International Power Electronics Conference (IPEC)*, Niigata, Japan, May 2018, pp. 2668–2672.

[11] G. P. Incremona, M. Cucuzzella, A. Ferrara, and L. Magni, "Model predictive control and sliding mode control for current sharing in microgrids," in *2017 IEEE 56th Annual Conference on Decision and Control (CDC)*, Melbourne, VIC, Australia, Dec. 2017, pp. 2661–2666.

[12] M. Cucuzzella, S. Trip, A. Ferrara, and J. Scherpen, "Cooperative voltage control in ac microgrids," in *Proc. IEEE Conference on Decision and Control (CDC)*, Miami Beach, Florida, USA, Dec. 2018, pp. 6723–6728.

[13] S. Trip, M. Cucuzzella, X. Cheng, and J. Scherpen, "Distributed averaging control for voltage regulation and current sharing in dc microgrids," *IEEE Control Systems Letters*, vol. 3, no. 1, pp. 174–179, Jan. 2019.

[14] A. Ferrara, G. P. Incremona, and M. Cucuzzella, *Advanced and Optimization Based Sliding Mode Control: Theory and Applications*. Philadelphia, PA: Society for Industrial and Applied Mathematics, 2019.

[15] A. Levant, "Higher-order sliding modes, differentiation and output-feedback control," *International Journal of Control*, vol. 76, no. 9, pp. 427–434, Sep. 2003.

[16] F. Dinuzzo and A. Ferrara, "Higher order sliding mode controllers with optimal reaching," *IEEE Transactions on Automatic Control*, vol. 54, no. 9, pp. 2126–2136, Sep. 2009.

[17] G. Bartolini, A. Ferrara, and E. Usai, "Chattering avoidance by second-order sliding mode control," *IEEE Transactions on Automatic Control*, vol. 43, no. 2, pp. 241–246, Feb. 1998.

[18] G. P. Incremona, M. Cucuzzella, and A. Ferrara, "Adaptive suboptimal second-order sliding mode control for microgrids," *International Journal of Control*, vol. 89, no. 9, pp. 1849–1867, Jan. 2016.